The International Journal of Advanced Manufacturing Technology (2023) 124:3601–3613
https://doi.org/10.1007/s00170-022-10655-9

ORIGINAL ARTICLE

Investigation of chip formation of Ti–6Al–4V in oxygen-free atmosphere

Berend Denkena[1] · Benjamin Bergmann[1] · Florian Schaper[1]

Received: 11 July 2022 / Accepted: 3 December 2022 / Published online: 11 January 2023

Abstract
Titanium and titanium alloys have high strength at low density, good corrosion resistance and excellent biocompatibility. Therefore, the use of titanium materials is well established in high-performance applications such as aerospace and biomedical. However, titanium and titanium alloys such as Ti–6Al–4 V have low thermal conductivity, exhibit unfavorable chip formation with typical segmented chips and have high chemical affinity to surrounding elements such as oxygen. Tool wear and the properties of the component surface and sub-surface are significantly influenced by the presence of oxygen and resulting chemical interactions. Among other things, chemical reactions such as oxidation occur due to the high temperatures and presence of oxygen. In this work, the chip formation of Ti–6Al–4 V at different cutting speeds in discontinuous orthogonal cutting process under different atmospheres is investigated. A conventional air atmosphere, a pure argon atmosphere and a silane-doped atmosphere were used. The oxygen content of the silane-doped argon atmosphere corresponds to an extremely high vacuum (XHV), which is practically oxygen-free. It was found that chip formation is affected by the surrounding atmosphere. At the cutting speed $v_c = 80$ m/min, non-periodic segmentation is present under oxygen-free atmosphere, while segmental chip formation occurs under air. This is accompanied by up to 16.5% lower feed force under inert gas atmosphere, which is due to reduced friction caused by the use of an oxygen-free atmosphere.

Keywords Cutting · Oxygen · Titanium · Chip formation

1 Introduction

Titanium and titanium alloys such as Ti–6Al–4 V are widely used in high-performance applications such as medical and aerospace due to outstanding mechanical properties with low density, a low corrosion tendency and high biocompatibility [1–3]. For the production of components made of Ti–6Al–4 V, cutting is of high relevance. During the cutting process, high temperatures occur in the area of the contact zone of the component and tool due to the material shear, favored by the low thermal conductivity of Ti–6Al–4 V [4]. Segmented chip formation is characteristic for the machining of titanium and titanium alloys, which has already been investigated in many studies [5–13]. Various models exist to explain segmentation of the titanium chip. One model is based on the generation of adiabatic shear bands due to the low thermal conductivity of titanium as a cause for chip segmentation. This is also favored by heat accumulation due to the low thermal conductivity of titanium. It results in thermal softening of the titanium at cyclic intervals, causing it to shear along the shear plane [8, 9, 14, 15]. However, investigations of titanium chips produced at cutting speeds below 1 m/min also reveal segmentation. Here it is assumed that thermal effects can be neglected. Cyclic crack initiation is used here as a model to describe the chip segmentation, where an occurrence of microcracks occurs at cyclic intervals. In this model, material shearing is the result of mechanical softening after the occurrence of a crack along the shear plane [6, 11, 16]. Vyas et al. divide the total energy that must be applied to chip formation into the specific energy to produce macroscopic cracks, microscopic cracks and friction of the chip against the rake face of the tool [11]. The friction process during chip formation can be divided into sticking and sliding friction [17]. The consequence of a segmented chip is a high-frequency thermomechanical alternating load on the cutting tool. Therefore, segmented chip formation

✉ Florian Schaper
schaper@ifw.uni-hannover.de

[1] Institute of Production Engineering and Machine Tools, Leibniz University Hannover, An der Universität 2, 30823 Garbsen, Germany

can be used as a significant factor for the high tool wear during the cutting of Ti–6Al–4 V [18, 19]. In addition, chip formation significantly affects the component surface and subsurface properties [9, 20, 21].

In [22] it was found that in external longitudinal turning of Ti–6Al–4 V with different coated and uncoated carbide tools lead to reduced wear due to decreasing oxygen content. In particular, this is attributed to a reduction in oxidation wear. In contrast, an increased adhesion is found through the use of an inert gas atmosphere [23]. The increased adhesion under inert gas atmosphere is confirmed by the studies of Mercer et al. by using argon in pin-on-disc-tests [24]. Ernst and Merchant found that the friction between the chip and the material is in strong interaction with the chip formation [25]. Reduced friction on the rake face during titanium cutting allows higher shear angles to be achieved, resulting in lower strain and lower process forces [9]. Bushlya et al. have used various cutting material-workpiece material pairings in machining under reduced ambient oxygen conditions. According to them, the effect of oxygen on the friction between chip and tool depends on the material pairing. Friction is increased for machining Inconel 718 with PcBN and reduced for the cutting from 34CrNiMo6 with cemented carbide and cermet as well as for the cutting of tool steel with PcBN due to oxide layer formation [26].

Williams et al. have investigated the influence of oxygen on the chip formation of different materials. While the presence of oxygen has a positive effect on the machining of iron-based materials, higher process forces occur for copper and aluminum as a result of the presence of oxygen [27]. However, no scientific work is known that investigates the chip formation of titanium and titanium alloys by reducing oxygen to an XHV-adequate atmosphere.

Furthermore, a large number of chemical and thermodynamic processes occur during the cutting process, which interact with each other and can influence the chip formation process. For example, diffusion processes can cause cutting material as well as oxygen, nitrogen and carbon from the ambient atmosphere or cutting fluid to penetrate the titanium chip or the workpiece surface [28–30]. Moreover, under high temperatures, aluminum and vanadium diffusion out of the Ti–6Al–4 V alloy occurs, as well as oxygen diffusion into the alloy through the oxide layer [31]. Titanium already forms an oxide layer at low temperatures, which has a passivating effect and thus prevents further oxidation of the titanium. However, at temperatures above 500 °C, the oxidation resistance decreases significantly, so that titanium has a much higher solubility for foreign elements such as O, N, C and H, which can change the material properties [32, 33]. These interstitially dissolved atoms and reaction products significantly affect the microstructure of titanium and its mechanical properties. Both, the reaction product TiO_2 and dissolved oxygen in alpha titanium, lead to an increase in hardness and shear strength compared to pure titanium [34, 35]. However, this is offset by an embrittlement effect due to the dissolution of oxygen in titanium [35, 36]. In addition, interstitial oxygen increases the grain size of the microstructure and thus increases the possibility of crack initiation of titanium materials [37]. Hartung et al. also observed the formation of reaction layers in the presence of oxygen during machining, which act as a barrier to diffusion between the cutting material and the titanium material [38].

To avoid oxidation during the cutting process, the significant reduction of oxygen is necessary. In order to be able to evaluate the results of the tests under reduced oxygen content, reference tests are first carried out under conventional air. Under air, the oxygen partial pressure is $p_{O2} = 212.28$ mbar [39]. Furthermore, an inert gas atmosphere with pure argon is used. According to the manufacturer, this has a maximum residual oxygen content of $p_{O2} = 2 \cdot 10^{-3}$ mbar. The monolayer formation time can be used to assess the oxygen adhesion dependent on the oxygen partial pressure. The absorption rate of oxygen molecules from the ambient atmosphere can be calculated as a function of the oxygen partial pressure. The gas molecules impinging per square centimeter j can be calculated according to Eq. (1), where p is the pressure in Pa, m_{O2} is the weight of the oxygen molecule, k_b is the Boltzmann constant and T is the absolute temperature.

$$j = p \cdot \sqrt{\frac{1}{\pi \cdot m_{O2} \cdot 2 \cdot k_b \cdot T}} \tag{1}$$

The number of $8.71 \cdot 10^{14}$ oxygen molecules on an area of 1 cm^2 forms a monolayer. Taking into account the sticking coefficient of 0.8 for oxygen on a titanium surface, the time for the formation of a monolayer t_{mono} for the absorption of oxygen on the surface is given by Eq. (2).

$$t_{mono} = \frac{8.71 \cdot 10^{14}}{0.8 \cdot j} \tag{2}$$

[40–42]. For the argon atmosphere, a monolayer formation time of $t_{mono} = 3.6 \cdot 10^{-5}$ s results. In order to achieve a practical freedom from oxygen, an atmosphere is aimed at which corresponds to an extremely high vacuum (XHV) with respect to the oxygen partial pressure. Below $p_{O2} = 10^{-11}$ mbar, oxygen partial pressures are considered XHV adequate [43]. This corresponds to a monolayer formation time of $t_{mono} = 7.2 \cdot 10^3$ s = 2 h. To achieve this, the gas monosilane SiH_4 is additionally added to the argon. This reacts with the remaining atmospheric oxygen to form silicon dioxide and water or hydrogen $SiH_4 + 2O_2 \rightarrow SiO_2 + 2H_2O$ and $SiH_4 + O_2 \rightarrow SiO_2 + 2H_2$ [44].

In this paper, the influence of the atmosphere on the chip formation of the titanium alloy Ti–6Al–4 V is considered.

An innovative methodology has been applied. By using an oxygen sensor for the first time during cutting processes, the oxygen partial pressure is quantified. Moreover, by adding monosilane, the oxygen partial pressure can be reduced to a desired value in a targeted manner for the first time. The aim of this paper is to gain knowledge about the influence of oxygen on the chip formation of Ti–6Al–4 V in orthogonal cutting. Three atmospheres, each with a different oxygen content, are used to determine this influence. The results of the cutting tests with regard to chip formation of Ti–6Al–4 V under conventional air, oxygen-reduced argon „ “and oxygen-free silandoped argon are compared. The silane-doped argon atmosphere has such a low oxygen partial pressure that this atmosphere has the level of an XHV.

2 Experimental setup and methodology

2.1 Experimental setup

For the generation of the different cutting atmospheres, a gas-tight enclosure is installed in a vertical lathe by Gildemeister GmbH of the type CTV 400. The entire process chamber is shown in Fig. 1. The enclosure is connected on the one hand to the tool magazine of the lathe and on the other hand to the spindle. The translatory axis movements of the spindle can be realized by a special bellow. In addition to a gas supply, the process chamber has overpressure valves and an exhaust connection. Furthermore, a tool and workpiece change can be realized via a sluice system that can be flushed and exhausted separately, without changing the atmosphere. Gloves are integrated into the chamber for handling inside the gas tight process chamber.

A detailed illustration of the test setup can be seen in Fig. 2. A steel shaft is clamped on one side in the three-jaw chuck of the lathe. The workpiece, consisting of a sheet of Ti–6Al–4 V, is attached to this shaft via screw connections. The grooves introduced into the workpiece cause a discontinuous cut with four interventions per workpiece revolution and a relative engagement of 63%. In combination with the holes, a sudden interruption of the cut is effected. A detailed description of the principle is given in [45].

The cutting tool is fixed to a Kistler type 9129AA multicomponent dynamometer via a special clamp. The gas is added via a gas inlet directly into the effective contact zone of the cutting process. Similarly, the sample gas is tapped close to the effective zone. The sample gas is extracted from the test chamber by a pump via a volume flow of 25 l/h and passed through a lambda probe from mesa GmbH. The lambda probe converts the oxygen partial pressure into a voltage signal and is used for process-parallel monitoring of the oxygen partial pressure.

The cutting tool is an SNMA 120,408 indexable insert made of uncoated cemented carbide from Kennametal. The tool is clamped by a special holder in such a way that the rake angle is $\gamma = -6°$ and the clearance angle is $\alpha = 6°$. The cutting edge rounding of the tools is measured with an Alicona InfiniteFocus G5 measuring device and is $\overline{S} = 5 \pm 1$ µm. These data are summarized in Table 1.

Sheets of titanium alloy Ti–6Al–4 V of thickness 3 mm are used as test material. The chemical composition of the alloy is listed in Table 2.

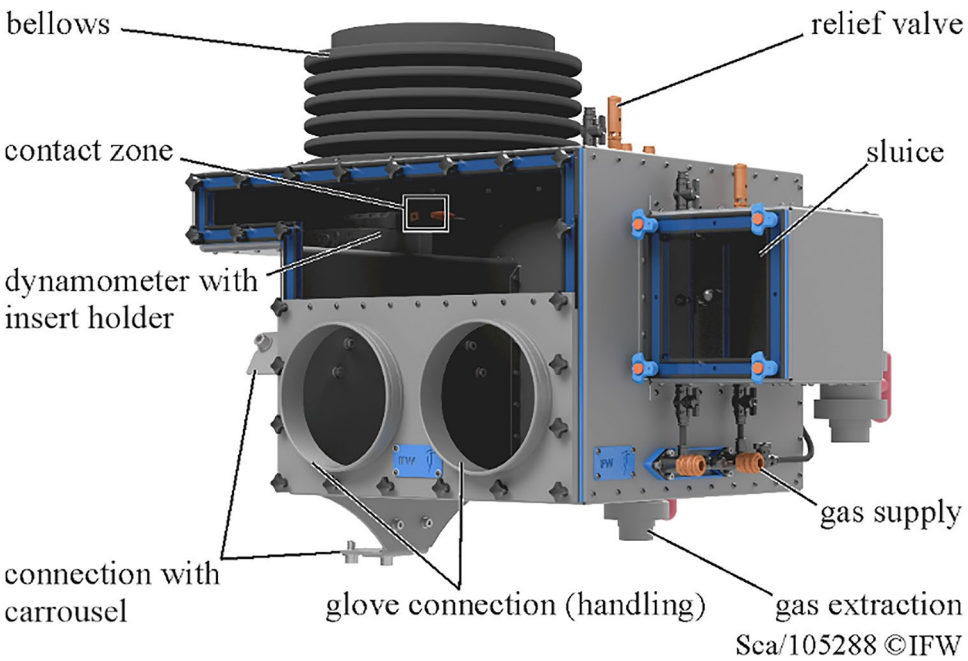

Fig. 1 Process chamber for the realization of different cutting atmospheres

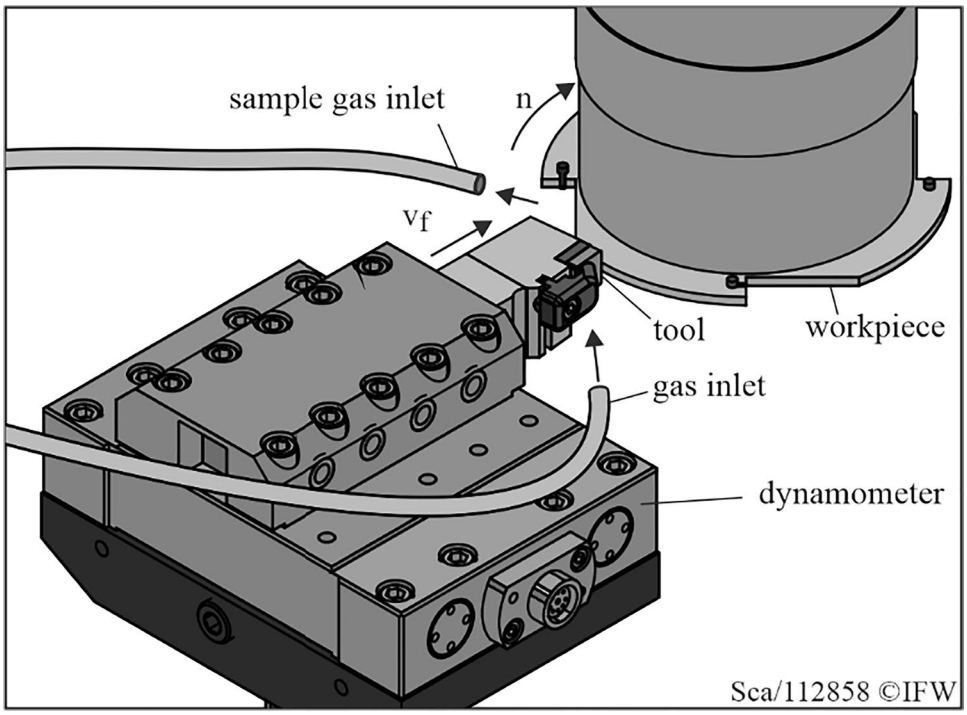

Fig. 2 Experimental setup inside the process chamber for the discontinuous orthogonal cutting process

Table 1 Micro and macro geometry of the test tools

Geometry	Rake angle γ	Clearance angle α	Cutting edge rounding $\overline{S}$
SNMA 120,408	−6°	6°	5 ± 1 µm

The most important mechanical properties of the material can also be found in Table 3.

The scanning electron microscope type Carl Zeiss EVO 60 is used for the scanning electron images to characterize the chips. Furthermore, the chip roots are cleaned with ethanol, ground with SiC abrasive paper and polished with Al_2O_3 abrasives. Subsequently, an etching process is performed with a water-based etchant containing 20% nitric acid and 2% hydrofluoric acid. The prepared chip roots are measured by light microscopy.

Table 3 Mechanical properties of Ti–6Al–4 V according to manufacturer

Yield strength R_{P02} [MPa]	Tensile strength R_m [MPa]	Elongation at break A [-]	Modulus of elasticity E [GPa]
828	892	10	110

2.2 Methodology of oxygen-free machining

A specific process strategy is required to generate the test atmospheres. The gases air, argon and a mixture of vol.-98.5% argon and vol.-1.5% monosilane are introduced via the gas supply of the process chamber. In addition, for the test atmospheres with reduced oxygen content, the spindle barrier air is substituted with argon. In this way, a continuous supply of unwanted oxygen is prevented and, at the same time, foreign particles such as silicon dioxide particles are prevented from entering the spindle.

Figure 3 shows the oxygen partial pressure over the flushing time of the different gases. Furthermore, the corresponding function of the monolayer formation time can be taken from Fig. 3. It can be seen that the oxygen content falls below the level of an XHV with $p_{O2} = 10^{-11}$ mbar after 41 min. The oxygen partial pressure of $p_{O2} = 10^{-17}$ mbar is defined as the experimental atmosphere in this paper and is reached after approx. 55 min of total flushing time. Due to mixing effects, flushing with argon takes up a large proportion of the time. There is always a slight overpressure, so that the

Table 2 Composition wt% of Grade 5 Ti–6Al–4 V

Wt.-%	Al	V	Fe	H	C	O	N	Ti
Min	5.5	3.5	0	0	0	0	0	Balance
Max	6.75	4.5	0.4	0.015	0.08	0.2	0.05	

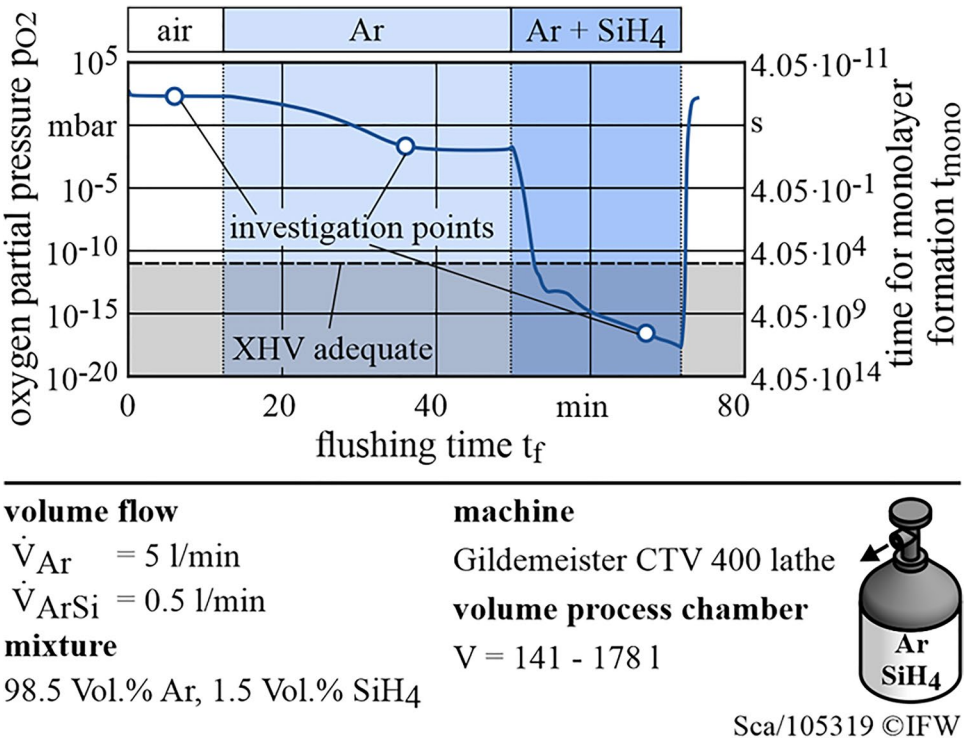

Fig. 3 Generation of the XHV adequate atmosphere and corresponding monolayer formation time

oxygen-containing gas mixture can be removed without drawing in fresh air.

Furthermore, the non-productive times of the process increase significantly. By stretching the bellows, which is firmly connected to the process chamber but also to the spindle, the volume of the process chamber is increased. The maximum speed of the spindle must be designed in such a way that the coupled increase in volume of the working chamber is always smaller than the gas flow supplied.

3 Results and discussion

3.1 Metallographical chip analysis

Chip roots are created by the principle of interrupting the cut. In this way, microscopic observation of the chip formation state is possible, which is highly dynamic in the process. Figure 5 illustrates the chip roots generated at $v_c = 80$ m/min in all three test atmospheres. A biaxial stress mode is present in the central region of the chip. The description of the process kinematics can therefore be two-dimensional in this region. In the lateral edge region of the chip, however, a triaxial stress mode exists. Therefore, the cross-section micrographs are generated in a manner that the lateral edge region of the chip is not considered. This is how the micrographs in Fig. 4 have been generated. From the cross-section micrographs it can be seen that the oxygen content influences the chip formation in the area of the chip midsection. While at $v_c = 80$ m/min in air there is a typical, almost periodic chip segmentation, the uniform segmentation decreases more and more due to the reduced oxygen content. The chip formation observed under XHV-equivalent argon-silane atmosphere can thus be classified as non-periodic segmented for this cutting speed. This chip formation resembles flow chip formation, since no shear localizations are formed.

The principle of not considering the edge regions of the chip in the evaluation can also be transferred from the chip roots to all other regions of the chip. Figure 5 illustrates this principle for each further chip that is not connected to a chip root. The SEM scans on the left also show where the transition from the lateral edge region of the chip to the middle region of the chip is to be located.

Geometric parameters can be derived from the cross-section micrographs of the chip roots shown in Fig. 4 and the cross-section images of the chips shown in Fig. 5. These are the degree of segmentation GS, the segment shear angle φ_s and the segmentation frequency f_s. The segment shear angle is derived directly from the courses of the shear localizations. The degree of segmentation can be calculated from the maximum chip thickness h'_{max} and the minimum chip thickness h'_{min} according to Eq. (3).

$$GS = \frac{h'_{max} - h'_{max}}{h'_{max}} \tag{3}$$

The segmentation frequency is calculated from the micrographs of the chips according to Eq. (4) [13]. It is assumed

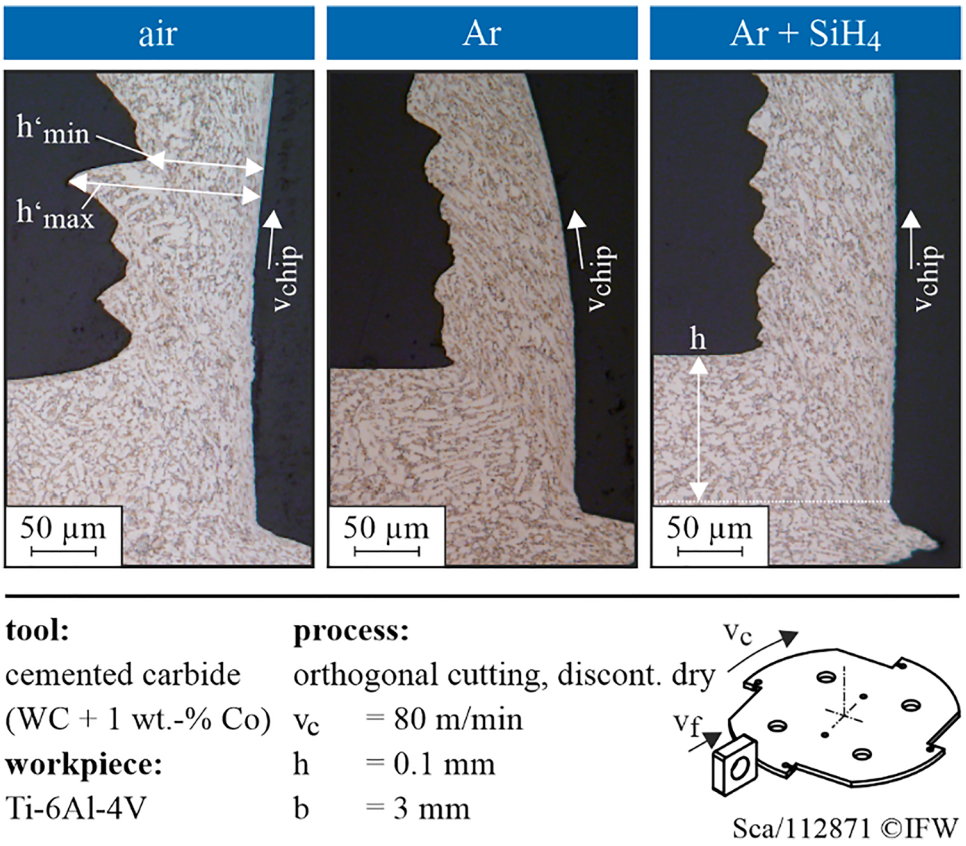

Fig. 4 Cross sections of the chip roots

that the average chip thickness h' corresponds to the mean value of the minimum and maximum chip thickness

$$f_s = \frac{1000 \cdot v_c \cdot h}{60 \cdot h' \cdot e_1} \tag{4}$$

where h is the undeformed chip thickness and e_1 is the length of a segment along the direction of chip flow on the rake face.

For the chip formation of Ti–6Al–4 V at a cutting speed of $v_c = 80$ m/min, the decrease of the oxygen content by using pure argon atmosphere causes a significant decrease in the degree of segmentation in the biaxial stress state, compared to the chips produced under air. Since there is no periodic segmentation at $v_c = 80$ m/min under argon and under silane-doped argon, the evaluation of the segment shear angle is not possible. It is also not possible to calculate the segmentation frequency in the case of non-periodic segmentation because the zones of shear localization are not clearly identifiable for this type of chip formation. Furthermore, the irregularity of the shear causes a strong variance of the segmentation frequency. In addition, the clear differentiation between shear localization as well as associated segments and a wavy surface is difficult. Similarly, identification of segment length along the chip flow direction is not possible for non-periodic segmentation. For this reason, it is also not possible to quantify the segmentation frequency in these cases.

3.2 Influence of the cutting speed

Increasing the cutting speed to 100 m/min and 120 m/min does not change the fundamental principle of segmented chip formation when cutting Ti–6Al–4 V under air. However, when using the argon atmosphere and the silane-doped argon atmosphere, the increase in cutting speed leads to a change in chip formation. At a cutting speed of $v_c = 100$ m/min or higher, periodic segmentation occurs even under oxygen-reduced atmosphere. For this reason, chip formation is performed analogously to the executions of the chips produced at $v_c = 80$ m/min and characterized on the basis of the segment shear angle, the segmentation frequency and the degree of segmentation. The results are summarized in Fig. 6. The diagrams allow the comparison of the parameters at constant cutting speed and variation of the atmosphere.

When looking at the segment shear angle, it can be seen that this parameter is at an almost constant level for all cutting speeds with the chips produced under air. In comparison, the segment shear angle decreases when the cutting speed is reduced from by increasing the cutting speed when purging with pure argon. As already described, it is not possible to quantify the segment shear angle for chip formation at $v_c = 80$ m/min in silane-doped argon atmosphere. Nevertheless, it can be determined that the segment shear angle under argon and under an XHV-equivalent silane-doped

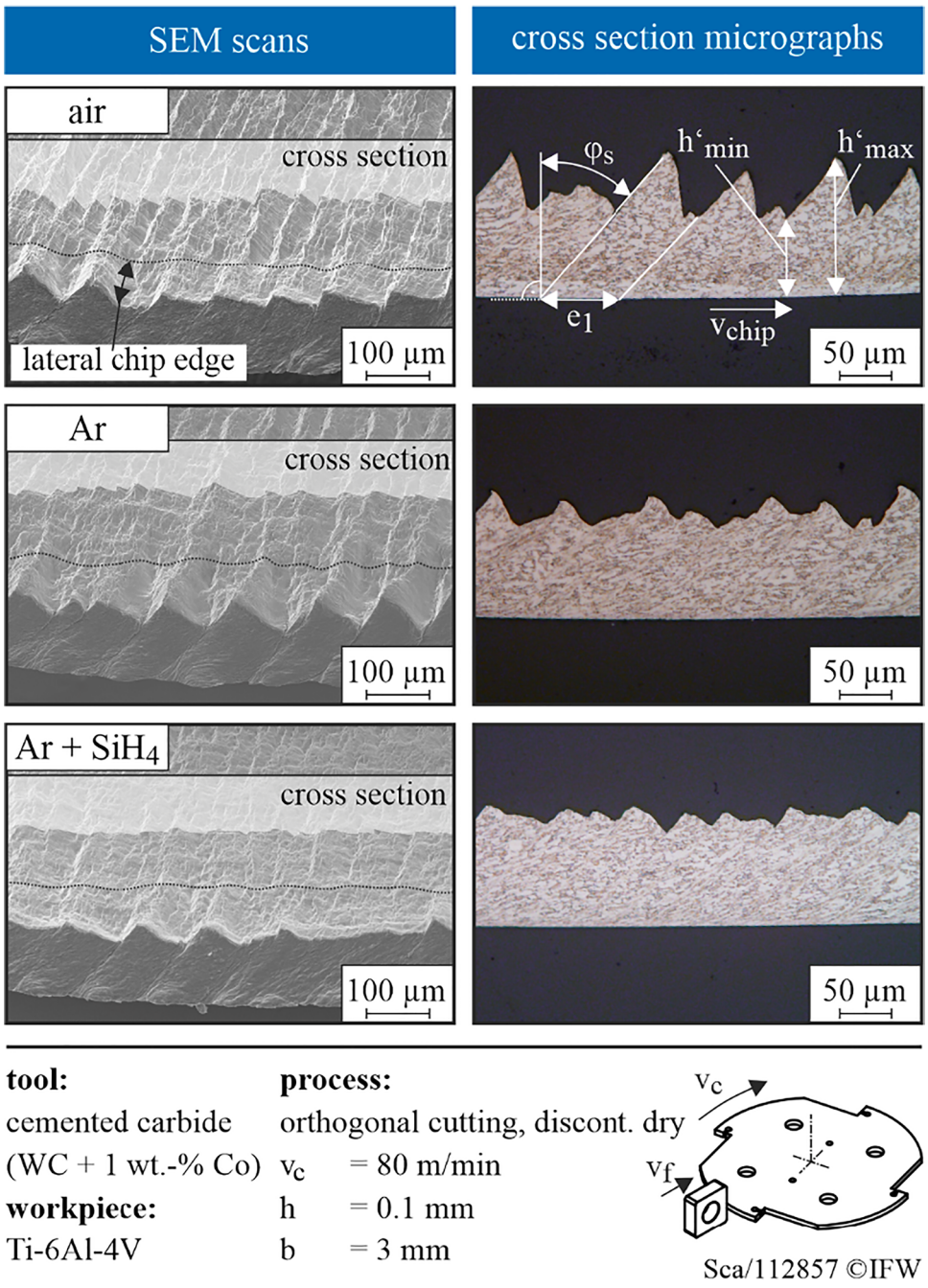

Fig. 5 Edge area, midsection and parameters in segmented chip formation

argon atmosphere decreases with increasing cutting speed. It can be observed that at $v_c = 100$ m/min, this parameter is 8% lower under XHV-equivalent atmosphere than under air, and at $v_c = 120$ m/min, the segment shear angle is even 44% lower.

With regard to the segmentation frequency, it becomes clear that lowering the oxygen content to XHV level causes a general increase in the segmentation frequency. At $v_c = 80$ m/min, analogous to the comments on the segment shear angle, the use of the segmentation frequency is not possible for the non-periodic segmented chips, formed in argon and silane-doped argon. At the cutting speed of 100 m/min, the segmentation frequency in an atmosphere suitable for XHV is 7% higher than in air, at $v_c = 120$ m/min, this parameter is 4% higher.

The course of the degree of segmentation is inverse to that of the segment shear angle. The degree of segmentation is generally at a constant level when using the air atmosphere. In contrast, the reduction of the oxygen content to XHV level causes an increase from 0.172 to 0.38, i.e. by

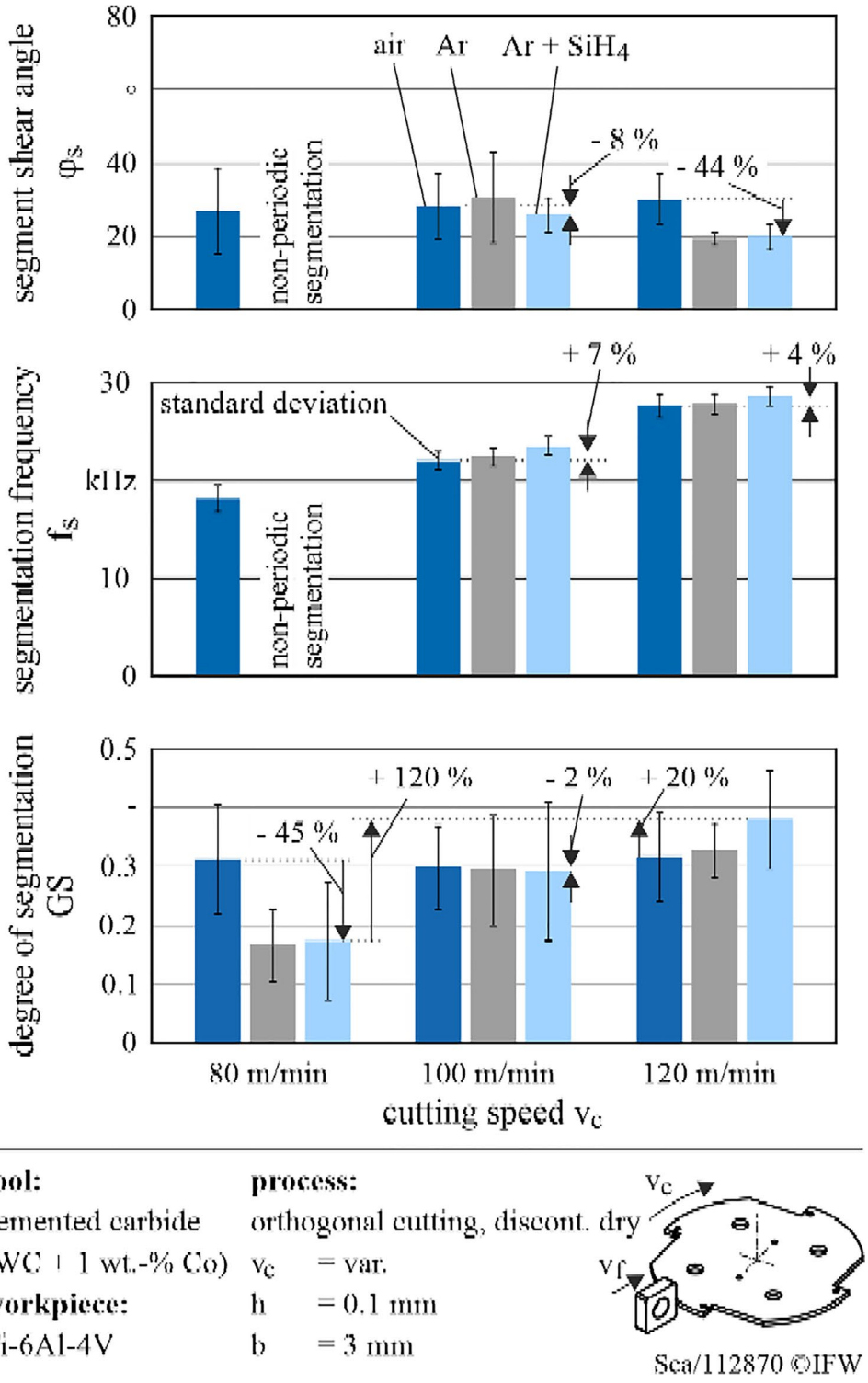

Fig. 6 Segmentation frequency and degree of segmentation depending on cutting speed and atmosphere

120%. Thus, the degree of segmentation is 45% lower at $v_c = 80$ m/min under silane-doped argon atmosphere, 2% lower at $v_c = 100$ m/min and.

20% higher at $v_c = 120$ m/min, in each case compared to the degree of segmentation under air. When using this parameter, the non-periodic segmentation at the cutting speed $v_c = 80$ m/min under argon and silane-doped argon must also be taken into account. However, since there is no ideal flow chip formation but non-periodic segmentation, this parameter is also used for characterization in these cases. This is supported by the fact that the degree of segmentation does not contain any information regarding the periodicity of the segmentation.

The results suggest that at a cutting speed of 80 m/min, the use of the XHV adequate atmosphere leads to a lower cyclic mechanical stress on the cutting edge due to chip segmentation. While periodic segmented chip formation is observed under air, the reduction in oxygen content results in non-periodic, weakened segmentation. This results in a significantly reduced degree of segmentation. In addition, the segments are formed at a slightly higher frequency under a significantly higher segment shear angle. However, as already described, the quantification of the segmentation frequency and the segment shear angle can only be used to a limited extent due to the change in chip formation. At the cutting speed of 100 m/min, a very small decrease in the dynamic mechanical cutting edge load can be expected, since the chip is formed only slightly more at higher frequency, with a slightly lower degree of segmentation and a slightly smaller segment shear angle. Accordingly, at the cutting speed of 120 m/min, a higher dynamic cutting edge load can be expected due to the lower segment shear angle, the higher degree of segmentation and the higher segmentation frequency.

3.3 Analysis of process forces

To obtain an estimate of the mechanical cutting edge load, the process forces are measured in the discontinuous cut. Due to the process kinematics, the process forces are the cutting force F_c and the feed force F_f. The sampling frequency during the measurement is 44.1 kHz. Subsequently, the cutting force and the feed force are averaged over the duration of the engagement. Figure 7 shows the mean cutting forces and feed forces, each as a function of cutting speed and atmosphere.

It can be seen that the cutting force is not significantly influenced by the cutting speed and the atmosphere. The feed force, on the other hand, shows a greater dependence on the ambient atmosphere. A comparison of the feed forces under air and XHV-equivalent atmosphere for the respective

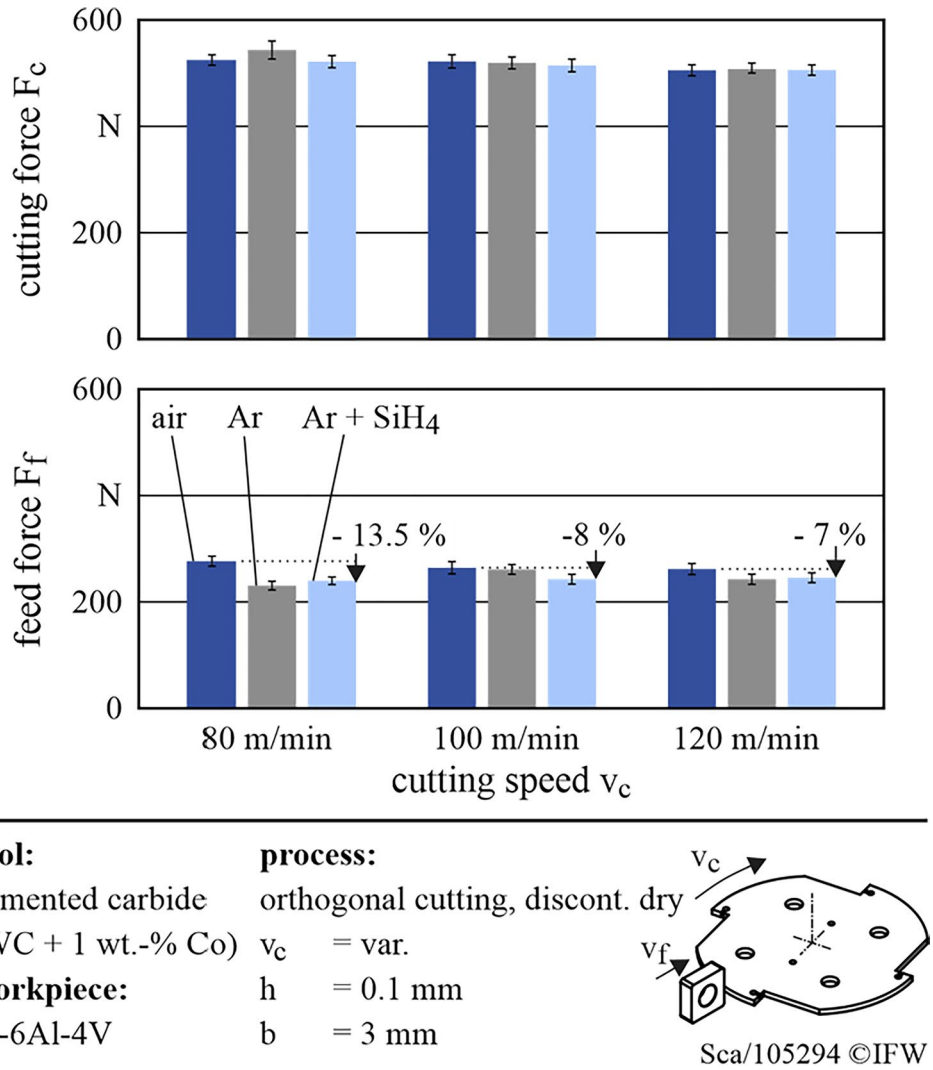

Fig. 7 Process forces depending on cutting speed and atmosphere

cutting speeds shows a reduction in the feed force of 13.5% at $v_c = 80$ m/min, an 8 = % lower value at $v_c = 100$ m/min and a 7% lower value at $v_c = 120$ m/min.

However, the reduction of the feed force by 13.5% for $v_c = 80$ m/min due to the lowering of the oxygen content is clearly above the measurement accuracy and thus to be classified as significant. Reducing the oxygen content by using argon and silane-doped argon causes non-periodic segmentation at $v_c = 80$ m/min. Contrary to expectations that this would lead to a significant reduction in the cutting speed, no significant difference is observed at this point. Presumably, this is due to the compensation of various effects by the absence of oxygen. It can be assumed that lower cutting temperatures are present under argon and silane-doped argon. This can be attributed to the non-periodic segmentation at $v_c = 80$ m/min under argon and silane-doped argon, while periodic segmentation is present under air. This approach can be explained by the model of adiabatic shear as the cause of the chip segmentation. At the same time, the expression of a non-periodic segmentation at $v_c = 80$ m/min is expected to result in a lower mechanical tool load. Lastly, a change in friction between the rake face and the chip as well as between the rake face and the workpiece surface can be expected. Furthermore, the effects mentioned above strongly interact with each other, which is why a separate consideration is difficult.

In contrast to the cutting force, the feed force decreases significantly as a result of the reduced oxygen content at $v_c = 80$ m/min. This is due to an atmospheric induced increase of the friction between the workpiece edge zone and the chip. The verification is performed by calculating the tangential force on the rake face $F_{t\gamma}$ and the normal force on the rake face $F_{n\gamma}$ for $v_c = 80$ m/min according to Eq. (5) and Eq. (6) [46].

$$F_{t\gamma} = F_f + F_c \cdot \tan\gamma \tag{5}$$

$$F_{n\gamma} = F_c - F_f \cdot \tan\gamma \tag{6}$$

This calculation, and also the use of Coulomb friction, is only valid for non-periodic segmentation without significant shear localization and is only an approximation for segmental chip formation under air. Furthermore, the friction at the clearance surface and at the cutting edge is neglected. However, the correlations show that under air there is a higher tangential force at the rake face than under argon and under silane-doped argon. This results in a 22% lower value under argon and a 16% lower value under silanized argon in the calculation of the coefficient of friction μ according to Eq. (7), compared to air. Figure 8 illustrates these quantities and their dependence on the atmosphere at $v_c = 80$ m/min.

$$\mu = \frac{F_{t\gamma}}{F_{n\gamma}} \tag{7}$$

The cutting speed and the friction between the chip and the tool significantly determine the heat input and the associated chip temperature. At a low cutting speed, the chip temperature is also lower. There is less friction between chip and tool in the silane-doped argon atmosphere than under air at $v_c = 80$ m/min. The consequence is a lower chip temperature and a lower feed force as well as a non-periodic chip segmentation result. During titanium cutting, high contact zone temperatures occur due to the low conductivity of titanium. Above this temperature of 500 °C, it can be considered that

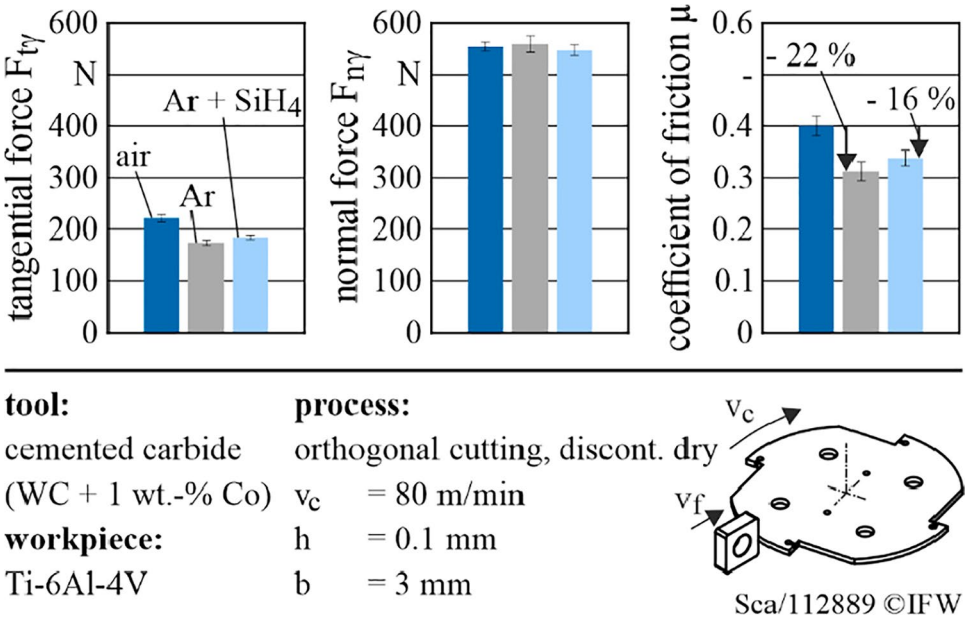

Fig. 8 Tangential force, normal force and coefficient of friction for non-periodic segmented chip formation

the titanium oxide layer formed has no passivating properties. Thus, it is assumed that the oxides in the contact zone contribute either directly to increased friction with the tool or even to increased friction due to third-body friction.

By increasing the cutting speed, several effects occur. First, the chip temperature increases for all atmospheres used. The result is periodic chip segmentation for all atmospheres at $v_c = 100$ m/min. Furthermore, in the presence of atmospheric oxygen, friction increases, which is why there is a significant increase in feed force when increasing from $v_c = 80$ m/min to $v_c = 100$ m/min while the cutting force remains almost constant. If the cutting speed increases further to $v_c = 120$ m/min, the effect of thermal material softening predominates under air, so that the feed force is reduced. In comparison, the feed force under argon and silane-doped argon increases slightly over the cutting speed range considered. The feed force in silane-doped argon atmosphere also shows an increase over the cutting speed range considered. In particular, in the range from $v_c = 100$ m/min to $v_c = 120$ m/min. Thus, there is a thermally induced increase in friction. It can be assumed that the temperatures under oxygen-reduced atmosphere are below air, so that in this range of the cutting speed thermal material softening does not contribute to the reduction of the feed force.

4 Conclusions and outlook

In this paper, the chip formation of titanium alloy Ti–6Al–4 V as a function of ambient atmosphere was investigated in dry discontinuous orthogonal cutting. The following conclusions can be drawn from the results:

1. The reduction of oxygen content by using a shielding gas atmosphere with silane-doped argon during discontinuous orthogonal cutting affects the chip formation of Ti–6Al–4 V. At a cutting speed of 80 m/min, the segmental chip formation typical of titanium occurs under air. This is in contrast to the non-periodic segmentation under oxygen-reduced and oxygen-free atmospheres, which resembles continuous flow chip formation.
2. The cutting force F_c in discontinuous cutting of Ti–6Al–4 V is not affected by the atmosphere and thus remains almost constant.
3. The feed force F_c is decreased by up to 16.5% by using oxygen-reduced atmospheres.
4. The reduced feed force with unchanged cutting force as well as the expression of different chip formation at $v_c = 80$ m/min is attributed to the reduction of friction between the tool and the chip by using the inert gas atmospheres. The adiabatic shear approach supports the significant influence of temperature on the expression of shear localization during segmental chip formation. A coefficient of friction up to 22% lower under inert gas atmosphere than under air can be observed.

The reduced contact zone temperature due to the lower friction between chip and rake face in oxygen-free titanium cutting significantly influences chip formation. In addition, the temperature has a significant influence on the oxide formation of the titanium and the passivation properties. The quantification of contact zone temperatures is therefore an important investigation that follows on from the results of this paper.

Furthermore, it can be assumed that there is an influence of the atmosphere on the surface quality and subsurface properties of the titanium component. This may be due to the surface chemical reactions and thermal stress. Investigations in this regard therefore also follow the explanations given in this paper.

Author contribution All authors contributed to the study conception and design. The experimental work and the theoretical analysis were performed by FS. The manuscript was written by FS. BD acquired the funding for the project leading to this publication. BD and BB reviewed the manuscript. All authors read and approved the final manuscript.

Funding Open Access funding enabled and organized by Projekt DEAL. Funded by the Deutsche Forschungsgemeinschaft (DFG, German Research Foundation)—Project-ID 394563137-SFB 1368 (TP-B03).

Data availability Available on request.

Code availability Not applicable.

Declarations

Ethics approval Not applicable.

Consent to participate Not applicable.

Consent for publication The manuscript is approved by all authors for publication; all the authors listed have approved the manuscript that is enclosed.

Conflict of interest The authors declare no competing interests.

References

1. Ratner BD (2001) A perspective on titanium biocompatibilty. In: Brunette D, Tengcall P, Textor M, Thomsen P (ed) Titanium in medicine. Springer Verlag, Berlin Heidelberg. https://doi.org/10.1007/978-3-642-56486-4
2. Veiga C, Davim JP, Loureiro AJR (2012) Properties and applications of titanium alloys: a brief review. Rev Adv Mater Sci 2012(32):133–148
3. Williams JC, Boyer RR (2020) Opportunities and issues in the application of titanium alloys for aerospace components. Metals 10(6). p 705 (10). https://doi.org/10.3390/met10060705
4. Ezugwu EO, Wang ZM (1997) Titanium alloys and their machinability—a review. J Mater Process Technol 68(I):262–274. https://doi.org/10.1016/S0924-0136(96)00030-1
5. Gente A, Hoffmeister H-W, Evans CJ (2001) Chip formation in machining Ti6Al4V at extremely high cutting speeds. CIRP Ann 50(1):49–52. https://doi.org/10.1016/S0007-8506(07)62068-X
6. D. M. Turley (1981) Slow speed machining of Titanium. Materials Research Labs., Ascot Vale (Australia)
7. Komanduri R, Brown RH (1981) On the mechanics of chip segmentation in machining. J Eng Ind 103(1):33–51. https://doi.org/10.1115/1.3184458
8. Komanduri R, Turkovich BF (1981) New observations on the mechanism of chip formation when machining titanium alloys. Wear 69(2):179–188. https://doi.org/10.1016/0043-1648(81)90242-8
9. Komanduri R (1982) Some clarifications on the mechanics of chip formation when machining titanium alloys. Wear 76(1):15–34. https://doi.org/10.1016/0043-1648(82)90113-2
10. Nakayama K, Arai M, Kanda T (1988) Machining characteristics of hard materials. CIRP Ann 37(1):89–92. https://doi.org/10.1016/S0007-8506(07)61592-3
11. Vyas A, Shaw MC (1999) Mechanics of saw-tooth chip formation in metal cutting. J Manuf Sci Eng 121(2):163–172. https://doi.org/10.1115/1.2831200
12. Su GS, Liu ZQ (2011) The analysis of saw-tooth chip formation in high speed machining trough material micro-hardness measurement. Adv Mater Res 188:9–14. https://doi.org/10.4028/www.scientific.net/AMR.188.9. Accessed 27 2022
13. Hrechuk A, Bushlya V, M'Saoubi R, Stahl J-E (2019) Quantitative analysis of chip segmentation in machining using an automated image processing method. Procedia CIRP 82:314–319. https://doi.org/10.1016/j.procir.2019.03.272
14. Recht RF (1964) Catastrophic thermoplastic shear. J Appl Mech 31(2):189–193. https://doi.org/10.1115/1.3629585
15. Zhen-Bin H, Komanduri R (1995) On a thermomechanical model of shear instability in machining. CIRP Ann 44(1):69–73. https://doi.org/10.1016/S0007-8506(07)62277-X
16. Shaw MC (2005) Metal cutting principles, Oxford University Press, vol. 2, Issue 3, New York
17. Zorev NN (1963) Interrelationship between shear processes occurring along tool face and on shear plane in metal cutting. In International Production Engineering Research Conference - Proceedings, Am Soc Mech Eng (ASME), pp 42–49
18. Barry J, Byrne G, Lennon D (2001) Observations on chip formation and acoustic emission in machining Ti-6Al-4V alloy. Int J Mach Tools Manuf 41(7):1055–1070. https://doi.org/10.1016/S0890-6955(00)00096-1
19. Lindvall R, Lenrick F, Persson H, M'Saoubi R, Stahl J-E (2020) Performance and wear mechanisms of PCD and PcBN cutting tools during machining titanium alloy Ti6Al4V. Wear 454–455:203329. https://doi.org/10.1016/j.wear.2020.203329
20. Wang Z-M, Jia Y-F, Zhang X-C, Fu Y, Zhang C-C, Tu S-T (2019) Effects of different mechanical surface enhancement techniques on surface integrity and fatigue properties of Ti-6Al-4V: a review. Crit Rev Solid State Mater Sci 44(3):445–469. https://doi.org/10.1080/10408436.2018.1492368
21. Li X, Yang S, Lu Z, Zhang D, Zhang X, Xiangyu X (2020) Influence of ultrasonic peening cutting on surface integrity and fatigue behavior of Ti-6Al-4V specimens. J Mater Process Technol 275:1–8. https://doi.org/10.1016/j.jmatprotec.2019.116386
22. Denkena B, Dittrich M-A, Krödel A, Worpenberg S, Matthies J, Schaper F (2020) Wear behaviour of coated cemented carbide inserts in an oxygen-free atmosphere when machining Ti-6Al-4V. Defect Diffus Forum 404:28–35. https://doi.org/10.4028/www.scientific.net/DDF.404.28. Accessed 27 Dec 2022
23. Schaper F, Denkena B, Dittrich M-A, Krödel A, Matthies J, Worpenberg S (2021) Wear behaviour of PCBN, PCD, binderless PCBN and cemented carbide cutting inserts when machining Ti-6Al-4V in an oxygen-free atmosphere. Proceedings of the 10th Congress of the German Academic Association for Production Technology, pp. 275–283. https://doi.org/10.1007/978-3-662-62138-7_28
24. Mercer AP, Hutchings IM (1988) The influence of atmospheric composition on the abrasive wear of titanium and Ti-6Al-4V. Wear 124(2):165–176. https://doi.org/10.1016/0043-1648(88)90242-6
25. Ernst H, Merchant ME (1940) Chip formation, friction, and high quality machined surfaces. In American Society for Testing Materials - Preprint (N 53). Am Soc Testing Materials (ASTM), pp 299–337
26. Bushlya V, Lenrick F, Stahl J-E, M'Saoubi R (2018) Influence of oxygen on the tool wear in machining. CIRP Ann 67(1):79–82. https://doi.org/10.1016/j.cirp.2018.03.011
27. Williams JA, Stobbs WM (1979) Changes in mode of chip formation as function of presence of oxygen. Met Technol 6(1):424–432. https://doi.org/10.1179/030716979803276570
28. Bai D, Sun J, Wang K, Chen W (2018) Diffusion behavior and wear mechanism of WC/Co tools when machining of titanium alloy. Solid State Phenom 279:60–66. https://doi.org/10.4028/www.scientific.net/SSP.279.60. Accessed 27 Dec 2022
29. Child HC, Dalton AL (1968) Machining of titanium alloys, Part 1. ISI Special Report 94, London, pp 139–142
30. Denkena B, Krödel A, Pyzcak F, Rackel MW, Kettelmann S, Matthies J (2021) Recycled titanium chips as initial product for the atomisation process of powders for additive manufacturing to increase resource efficiency. In: Proceedings of 21st Machining Innovations Conference for Aerospace Industry, pp 89–97. https://doi.org/10.2139/ssrn.3936516
31. Dong E, Yu W, Cai Q, Cheng L, Shi J (2017) High-temperature oxidation kinetics and behavior of Ti-6Al-4V alloy. Oxid Met 88(5–6):719–732. https://doi.org/10.1007/s11085-017-9770-0
32. Donachie MJ (2000) Joining technology and practice. In: Donachie MJ (ed) Titanium: a technical guide. ASM International, Materials Park, pp 65–78. https://doi.org/10.31399/asm.tb.ttg2.t61120065
33. Kaplan Y, Cetin Can A, Ulukoy A (2019) A new medium for boriding of Ti6Al4V alloy for biomedical applications. Proc Inst Mech Eng Pt L J Mater Des Appl 233(2):109–119. https://doi.org/10.1177/1464420716662801
34. Buckley DH (1971) Friction, wear and lubrication in vacuum. NASA Scientific and Technical Publication SP – 277, Washington, D. C
35. Liu Z, Welsch G (1988) Effects of oxygen and heat treatment on the mechanical properties of alpha and beta titanium alloys. Metall Trans A 19(3):527–542. https://doi.org/10.1007/BF02649267
36. Buckley DH, Johnson RL (1966) Friction, wear and adhesion characteristics of titanium-aluminum alloys in vacuum, NASA Scientific and Technical Publication D - 3235. D. C, Washington
37. Yoder GR, Cooley LA, Crooker TW (1978) Fatigue crack propagation resistance of beta-annealed Ti-6Al-4V alloys of differing

interstitial oxygen contents, Metallurgical Transactions A 9:1413–1420. https://doi.org/10.1007/BF02661812
38. Hartung PD, Kramer BM, Turkovich BF (1982) Tool wear in titanium machining. CIRP Ann 31(1):75–80. https://doi.org/10.1016/S0007-8506(07)63272-7
39. Heicklen J (1976) Atmospheric chemistry. Academic Press, New York
40. Steinherz HA (1963) Handbook of high vacuum engineering. Reinhold Publishing Corporation, New York
41. Gustus R, Szarfarska M, Maus-Friedrichs W (2021) Oxygen-free transport of samples in silane-doped inert gas atmosphere for surface analysis. J Vac Sci Technol 39(5):054204. https://doi.org/10.1116/6.0001180
42. Harra DJ (1976) Review of sticking coefficients and sorption capacities of gases on titanium films. J Vac Sci Technol 13(1):471–474. https://doi.org/10.1116/1.568900
43. Redhead PA (1999) Extreme high vacuum,. In: Turner S (ed) Proceedings of CAS - CERN Accelerator School: Vac Technol, CERN, Snekersten, Denmark, pp 213–226. https://doi.org/10.5170/CERN-1999-005.213
44. Holländer U, Wulff D, Langohr A, Möhwald K, Maier H-J (2019) Brazing in SiH4-doped inert gases: a new approach to an environment friendly production process. Int J Precis Eng Manuf-Green Technol 7(6):1059–1071. https://doi.org/10.1007/s40684-019-00109-1
45. Tönshoff HK, Denkena B (2013) Chip formation. In: Tönshoff HK, Denkena B (ed) Basics of Cutting and Abrasive Processes, Springer Berlin Heidelberg, pp 21–36. https://doi.org/10.1007/978-3-642-33257-9_2
46. Merchant ME (1944) Basic mechanics of the metal-cutting process. J Appl Mech 11(3):168–175. https://doi.org/10.1115/1.4009380